Review Article

Advanced magnetic resonance imaging in the study of primary intracranial brain tumors in adults: a state of art review

Francesco Lavra[1], Mario Scartozzi[2], Fulvio Zaccagna[3], Gaia Cartocci[4], Luca Saba[1]

[1]Department of Radiology, [2]Department of Oncology, University of Cagliari, Cagliari, Italy; [3]Department of Radiology, University of Cambridge School of Clinical Medicine, Cambridge Biomedical Campus, Cambridge CB2 0QQ, UK; [4]Department of sanità Pubblica, Malattie Infettive e microbiologia, Università di Roma Sapienza, Piazzale Aldo Moro, Roma, Italy

Contributions: (I) Conception and design: F Lavra; (II) Administrative support: L Saba; (III) Provision of study materials or patients: All authors; (IV) Collection and assembly of data: F Lavra, L Saba; (V) Data analysis and interpretation: F Lavra; (VI) Manuscript writing: All authors; (VII) Final approval of manuscript: All authors.

Correspondence to: Luca Saba. Department of Radiology, University of Cagliari, Cagliari, Italy. Email: lucasabamd@gmail.com.

Abstract: Intracranial tumors are an important health problem with an annual incidence of primary and secondary central nervous system neoplasms ranges from 10 to 17 per 100,000 persons. Tumor imaging have as fundamental aims: the initial differential diagnosis with the distinction between newly diagnosed brain tumors and non-neoplastic lesions, ischemia, extra-axial neoplasm and metastasis; the preoperative planning, estimating the tumor grade, guiding the biopsy, resection, local ablative therapy and therapeutic follow-up; the monitoring of disease progression and therapeutic response, including the differentiation of recurrent tumor from delayed radiation necrosis. Imaging plays an integral role in intracranial tumor management. In particular, conventional magnetic resonance imaging (cMRI) has emerged as the imaging modality most frequently used to evaluate intracranial tumors offering important anatomic informations even though sometimes these anatomic informations are not exhaustive in the correct assessment of these tumors. In this review, we are going to investigate the role of the most widely available and practical techniques such as diffusion-weighted imaging (DWI), perfusion-weighted imaging MRI (PMR), diffusion-tensor imaging (DTI), and MR spectroscopy (MRS).

Keywords: Magnetic resonance imaging (MRI); intracranial neoplasms

Received: 10 April 2017; Accepted: 19 June 2017; Published: 19 July 2017.
doi: 10.21037/jxym.2017.06.01
View this article at: http://dx.doi.org/10.21037/jxym.2017.06.01

Introduction

Intracranial tumors are an important health problem with an annual incidence of primary and secondary central nervous system neoplasms ranges from 10 to 17 per 100,000 persons.

The annual incidence of malignant glioma is 5 per 100,000 (1) and patient with malignant glioma have a worse prognosis compared to those with a secondary brain tumor with a median survival of 15 months (2). The median survival of patients with a recurrent glioma is 3–6 months (3).

Tumor imaging have as fundamental aims: the initial differential diagnosis with the distinction between newly diagnosed brain tumors and non-neoplastic lesions, ischemia, extra-axial neoplasm and metastasis; the preoperative planning, estimating the tumor grade, guiding the biopsy, resection, local ablative therapy and therapeutic follow-up; the monitoring of disease progression and therapeutic response, including the differentiation of recurrent tumor from delayed radiation necrosis.

Imaging plays an integral role in intracranial tumor management. In particular, conventional magnetic resonance imaging (cMRI) (*Figure 1*) has emerged as the imaging modality most frequently used to evaluate intracranial tumors offering important anatomic informations even though sometimes these anatomic informations are not exhaustive in the correct assessment of

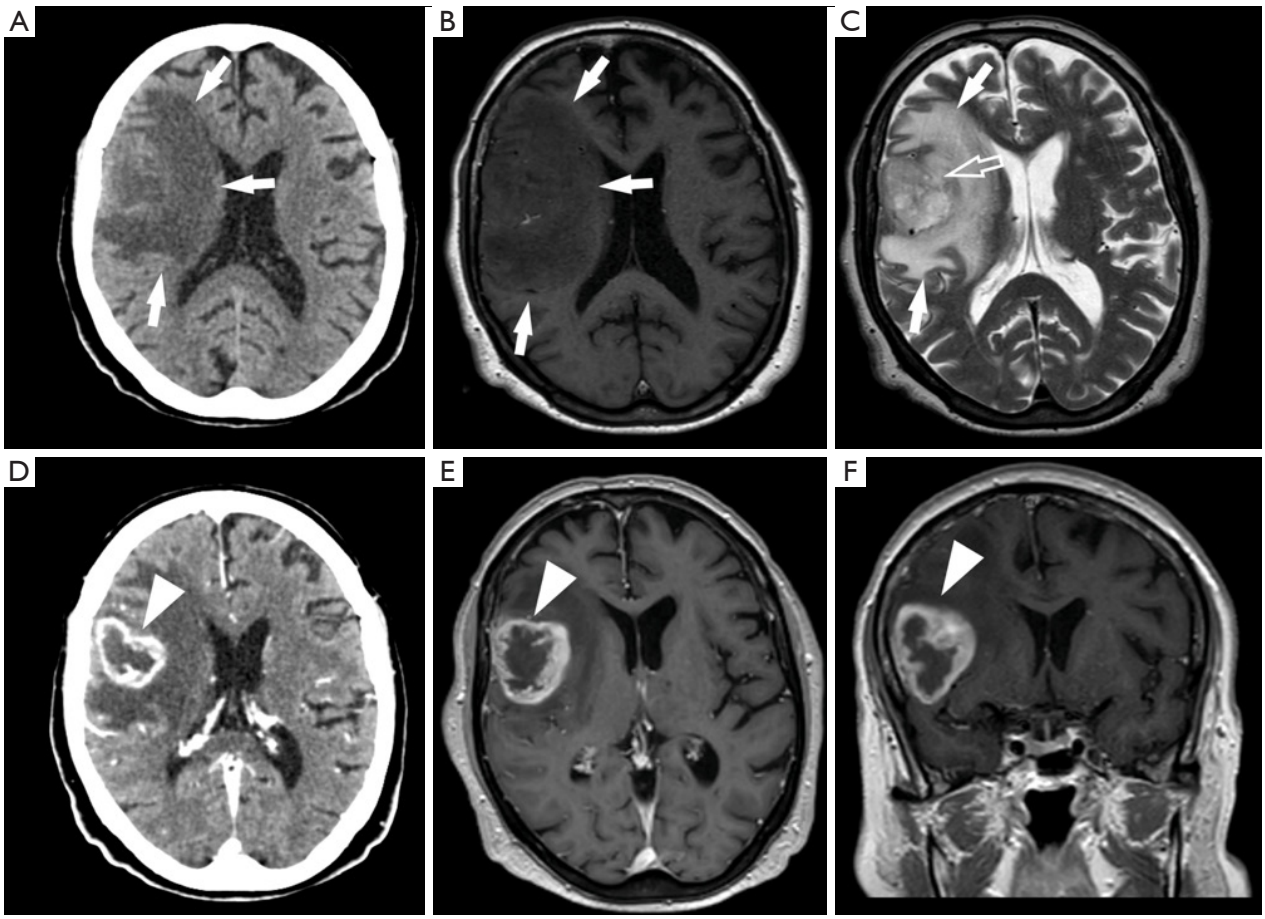

Figure 1 High-grade glioma in an 84-year-old female subject. CT axial (A) and MR (B,C) images without contrast material demonstrate the presence of an intracranial mass with edema. After administration of contrast material the CT (D) and MR (E,F) images show the contrast-enhancement of the lesion. CT, computed tomography; MR, magnetic resonance.

these tumors.

In addition to conventional MR imaging techniques, it has become in the clinical practice available a variety of advanced techniques that generate physiologic data, information on chemical composition which are very important for a proper assessment and prognosis definition of these tumors.

For these reasons, advanced magnetic resonance (aMR) techniques, have started to be widely used in clinical brain tumor imaging. These techniques are all adapted from, and must be interpreted in the context of conventional MRI techniques that provide image contrasts reflecting gross anatomy on a scale of 500 micron or greater (4).

In this review, we are going to investigate the role of the most widely available and practical techniques such as diffusion-weighted imaging (DWI), perfusion-weighted imaging MRI (PMR), diffusion-tensor imaging (DTI), and MR spectroscopy (MRS).

Advanced MRI techniques functioning

DWI

DWI contrast reflects the Brownian motion of tissue water.

The basic idea is to use paired magnetic-field gradients to "encode", and subsequently decode, the spatial motion of the molecules. Signal intensity is represented by the following equation:

$$s=0\times\exp\alpha\left(b\times ADC\right) \quad [1]$$

In this equation, ADC is the apparent diffusion coefficient (ADC) and b is the gradient factor, commonly referred to as the b-factor. It's above all that the b-value

affects the sensitivity to diffusion-based contrast.

S=0 is the signal intensity when no diffusion gradients are used. The ADC is an average of the diffusion process occurring in the tissues. According to this equation, the measured signal is reduced when diffusion gradients (b≠0) are applied.

As the diffusing spins move inside the field, they are affected differently by the field that spoils the alignment with each other. Since the measured signal is a summation of tiny signals from all individual spins, the misalignment, or "dephasing", caused by the gradient pulses results in a drop in signal intensity which is directly proportional to the diffusion distance. According to this equation, for a fixed b-factor, high ADC values translate to low signal. A parametric ADC map (ADC map) can be generated after the application of different b-values as well as one image with no b-weighting (often referred to as the 'b0 image'). The b-value is a factor that expresses the influence of the gradients on the diffusion-weighted images. Image intensities in the ADC map correspond to diffusion strength in the pixels (5).

The ADC in brain tissue is principally determined by tissue cellularity.

Diffusion tensor tractography (DTT)

Water molecules diffusion in a given direction at the cellular level in the brain is influenced by the myelin sheath covering neural axons; as a matter of fact, they diffuse more easily parallel to the WM tracts rather than perpendicular to them.

Diffusion tensor imaging (DTI) provides informations in a three-dimensional (3D) space on this directional variation of water molecules diffusion which is translated to a signal that is higher for diffusion-gradient encoding perpendicular to the WM tracts than parallel.

This directional variation in the signal intensity is termed "diffusion anisotropy" which we measure in each pixel using a matrix called "tensor" by acquiring DW images with at least six non-collinear gradient encoding directions. Then we define six parameters: λ1, λ2 and λ3, who are called eigenvalues and represent the magnitude of water molecules diffusion and three vectors v1, v2, and v3, who are called eigenvectors. These six parameters are determined from the six diffusion constant measurements or, in the other words, from the diffusion ellipsoid and the principle eigenvector (principle vector of diffusion ellipsoid) in each pixel represents the direction of greatest diffusion which also corresponds to the fiber tract axis.

This directional information allows to determine and represent the WM tract organization by using directionally color-coded schematic maps of major eigenvector orientation (6-9).

MRS

In a magnetic field, each proton nucleus has its own MR frequency resulting from the shielding by the surrounding covalent bond electron cloud. MRS tests the number of each chemically distinct proton (1H0) species present in each voxel by detecting slight differences in their NMR frequency ("chemical shift") and these differences are demonstrated on the abscissa of each graph (spectrum) in units of parts per million of the resonance frequency of a standard reference compound providing spectra that are comparable across field strength.

The ordinate of the graph represents arbitrary units of signal intensity scaled relative to the highest peak (10) being clinical MRS directly unquantifiable.

Two-dimensional (2D) or 3D MR spectroscopic imaging (2D-MRSI or 3D-MRSI, respectively) are referred to the simultaneous interrogation of 2D or 3D groups of small voxels and the data they provide can be used to produce impressive color "metabolite maps" that depict the spatial distribution of the different peak heights, areas, or peak ratios that can be derived from these spectra; these maps are not of common use for clinical diagnosis because the primary data can only be assessed from the spectral graphs.

The principal peaks seen in brain tumor MRS at 1.5 T include branch chain amino acids (0.9–1.0 ppm), lipid (0.9–1.5 ppm), lactate (1.3 ppm), alanine (1.5 ppm), n-acetylaspartate (NAA) (2.0 ppm), choline (3.2 ppm), creatine (3.0 and 3.9 ppm), and myoinositol (3.6 ppm).

NAA is a marker of neuronal number and function, creatine a marker of energy metabolism and stores, and choline a marker of membrane synthesis and degradation ("membrane turnover"). All processes that injure neurons decrease NAA; all processes that injure glia or stimulate glial division increase choline; all processes that disrupt aerobic glycolysis result in lactate formation; and all processes that produce necrosis release lipid and decrease creatine (11,12) (*Figure 2*).

Dynamic susceptibility T2-weighted perfusion (PMR)*

The high pressure injection of a large contrast dose is used

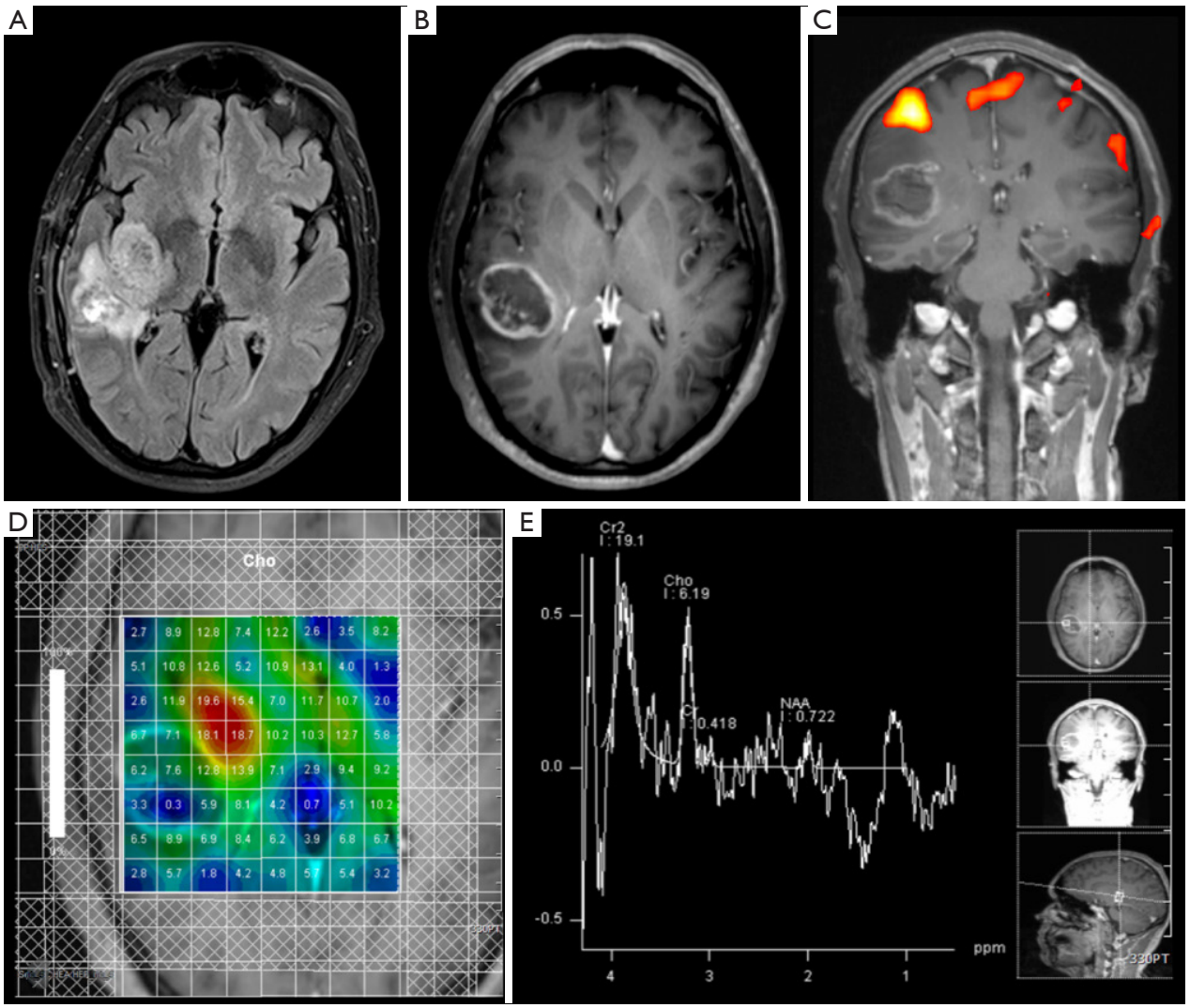

Figure 2 Right temporal lobe GBM: (A) axial T2 FLAIR; (B) axial T1 post gadolinium administration; (C) coronal BOLD showing motor activation; (D) axial multi-voxel MRS color-coded map of choline; and (E) spectra from a single voxel within the GBM. GBM, glioblastoma.

in the perfusion MRI to generate a dynamic drop in signal intensity on susceptibility (T2*)-weighted images acquired serially throughout the whole brain every 1 to 2 seconds during this injection.

We exploit the signal decrease in each voxel to compute the relative cerebral blood volume (rCBV) of that one, which can then be displayed as a color map or as a graph of the change in signal intensity in a given area over time [time-intensity curve (TIC)].

The blood volumes of normal-appearing white and gray matter are used as internal references for visual comparisons and for region-of-interest measurements (13) to produce relative blood volume maps.

To properly interpret these data, in addition to inspecting the rCBV maps, the check of the TIC is required to detect and account for magnetic susceptibility, motion, bolus timing, and other artifacts. The shape of the TIC provides a rough estimate of capillary permeability that can be very useful in differential diagnosis.

Dynamic contrast-enhanced T1 permeability imaging (T1P)

Fast-gradient echo-based T1-weighted images of the whole

brain acquired continuously from before the contrast bolus arrival until 2 to 3 minutes after injection are used to quantify the increase in signal intensity related to leakage of contrast agent from the intravascular compartment into the brain. This is the functioning base of the T1P imaging which is essentially a dynamic, semiquantitative adaptation of Gd-enhanced imaging.

Considering the lower temporal resolution and longer scan time, T1P is useful for imaging the steady state leakage of contrast during the first few phases of bolus recirculation, in contrast to dynamic susceptibility T2*-weighted perfusion, which images exclusively during the first pass.

We can exploit the TIC calculated from T1P to derive a number of parameters related to BBB impairment, the most widely reported of which is the net forward volume transfer constant (Ktrans) from the two-compartment pharmacokinetic modeling equation (4).

Advanced MRI in differential diagnosis of adult intra-axial brain tumors

Despite of being the most sensitive modality for the detection of brain tumors, cMRI has a low specificity and several different tumor types (as well as lesions of other etiologies) may share similar MRI features.

Low-grade gliomas and many non-neoplastic lesions, such as early stage lesions or diffusely infiltrating lesions, sometimes show no mass effect and low-grade gliomas may present as small T2 hyperintense lesions, that could be hard to discriminate from focal cortical dysplasias or other pathologies (14).

Since various non-neoplastic processes are often associated with blood-brain barrier disruption, and not all tumors enhance (15), sometimes the use of a contrast agent does not increase diagnostic specificity; infectious, ischemic or demyelinating lesions are examples of non-neoplastic lesions that can mimic brain tumors on cMRI (16).

Discriminating between extraaxial or intraaxial brain tumors is relatively easy with only anatomic imaging; however, the major diagnostic challenge is to reliably, noninvasively, and promptly differentiate intraaxial tumors to avoid biopsy and follow- up imaging studies.

Al-Okaili *et al.* (17) summarized the typical imaging features of the most common intracranial masses in adults—primary neoplasms (high-grade and low-grade), secondary (metastatic) neoplasms, lymphoma, tumefactive demyelinating lesions, abscesses, and encephalitis on perfusion MRI, diffusion MRI, and proton MR.

Primary (nonlymphomatous) neoplasms

MRS

The typical primary neoplasm features are elevated peaks of lipid, lactate, choline, and myoinositol and reduced NAA signal.

Unfortunately, the cutoff metabolite signal ratios that can frankly distinguish neoplastic from nonneoplastic conditions are not unequivocal. A choline/NAA ratio greater than 1 have showed a sensitivity of 79% and a specificity of 77% as an indicator of a neoplastic process. Using a logistical regression model with 10 input MR spectroscopic variables it was achieved a sensitivity of 87% and a specificity of 85% (18).

Despite of this fact Al-Okaili *et al.* found that a choline/NAA cutoff ratio of 2.2 does reliably separate high-grade from low-grade neoplasms and non-neoplastic conditions; high-grade neoplasms also tend to have elevated lipid signal, which is often absent in low-grade neoplasms.

On the other hand, a high myoinositol peak is more typical of lower grade neoplasms and gliomatosis cerebri (19).

DWI

A variable ADCs is the typical feature for primary neoplasms. Even though the ADC value of high-grade gliomas tend to be lower than that of low-grade gliomas (20), there is substantial overlap; thus, ADC map is not sufficient for predicting type and grade of glial neoplasms alone (21).

Perfusion imaging

A relative tumor blood volume (rTBV) that tends to increase with neoplasm grade is the typical perfusion imaging feature for primary neoplasms.

Neoplasms have increased permeability parameters because neoplastic-induced angiogenesis results in structurally abnormal vessels that tend to be leaky. The grade of the neoplasm correlates with tumor blood volume according to several studies (22,23); as a matter of fact, a rTBV value of 1.75 was indicated as a cutoff threshold to discriminate between a high grade from a low-grade neoplasm (22), where rTBV is a ratio of the maximal tumor blood volume to a region of interest in normal white matter (WM). On the other hand, low-grade glial neoplasms with oligodendroglial features, which may have markedly elevated rTBV are an exception (24): markedly elevated rTBV has been observed in particular in low-grade oligodendrogliomas and oligoastrocytomas with 1p deletion.

Secondary (metastatic) neoplasms

MRS

The typical secondary neoplasms features are elevated signals of lipid, lactate, and choline and reduced or absent NAA signal.

The utility of spectroscopic interrogation of the enhancing portion of the tumor to distinguishing metastases from high-grade primary neoplasm is poor, even though some results have shown the possibility to look for a higher degree of lipid signal in metastatic lesions (19,25). In contrast, it is useful to investigate the areas outside the enhancing portion of the lesion, considering that primary neoplasms have the propensity to infiltrate surrounding brain tissue (26,27). In fact, one study showed that a choline/NAA ratio of greater than 1 had an accuracy of 100% (26).

DWI

An elevated ADC is the typical feature for secondary neoplasms. Although there is a substantial overlap of ADC values between metastatic and primary brain neoplasm, it is possible to separate these two pathologies by measuring ADC values in the peritumoral regions.

Perfusion imaging

An elevated rTBV is the typical feature for secondary, metastatic lesions. As well as primary neoplasms, a crucial metastases ability is to induce angiogenesis for their growth. The perfusion parameters tend to overlap with those of high-grade neoplasms, probably because of their similarity in the degree of angiogenesis.

Metastatic lesions have lower rTBV measurements outside their enhancing portion, compared with those of the more infiltrative primary neoplasms and this feature may enable us to distinguish these two pathologies (27,28).

Lymphoma

MRS

Typical proton MR spectroscopic features for lymphoma include elevated signals of lipid, lactate, and choline and reduced NAA signal.

MRS of lymphoma in AIDS patients showed mild to moderately increased lactate and lipid signals, along with a prominent choline peak and decreased NAA, creatine, and myoinositol signals. This pattern can help in differentiating lymphoma from toxoplasmosis, which typically has elevated lactate and lipid signals but absence of the other metabolites in MR spectra (29).

DWI

A reduced ADC is the typical characteristic. Lymphoma is incline to have a low ADC due to its cellularity; thus, a low ADC value would favor lymphoma over glial tumors.

Perfusion imaging

The typical characteristic for lymphoma is a low rTBV compared with that of primary high-grade neoplasms.

The differentiation between lymphoma and primary high-grade glial neoplasms is feasible because lymphoma tends to have a lower rTBV (28), and the intensity time curves for lymphoma is substantially below the baseline (30).

Tumefactive demyelinating lesions

Acute monophasic syndromes enclose the Marburg variant of multiple sclerosis, Balo's concentric sclerosis, and other focal tumefactive demyelinating lesions that may mimic brain tumors.

MRS

The peculiar spectroscopic features are an elevated choline peak and reduced NAA signal.

A fulminant tumefactive demyelinating lesion may show high choline and low NAA signals as well as presence of lactate. Distinguishing a tumefactive demyelinating lesion from neoplastic lesions is often hard with MRS (31). In multiple sclerosis, the spectroscopic abnormalities were also shown in normal-appearing areas of WM that demonstrated to have reduced NAA signal (compared with NAA signals in healthy control subjects) although, in the early stages of the disease, it is less evident than an increased myoinositol peak.

DWI

The typical DWI feature is variable ADC. The majority of tumefactive demyelinating lesions show elevated ADC values, even though sometimes the acute ones may have areas of reduced ADC values (32).

Perfusion imaging

The typical perfusion imaging feature is low rTBV. In tumefactive demyelinating lesions, rTBV values tend to be lower than those in normal brain tissue, in high grade primary neoplasms and in metastatic lesions (28).

Brain abscesses

MRS

The typical spectroscopic characteristics are elevated peaks of amino acid, lactate, alanine, acetate, pyruvate, and succinate and absent signals of NAA, creatine, and choline.

Abscesses have a distinct spectroscopic pattern: for example, elevation of choline and absence of signal from a variety of amino acids, acetate, and succinate (33,34) would support a neoplastic process, whereas the other peaks listed above—alanine, acetate, pyruvate, and succinate—favor abscesses.

MRS may shed light on which organism is responsible for the abscess, because the presence of anaerobic bacteria tends to cause elevated acetate and succinate peaks, whereas absence of acetate and succinate signals are more probable with obligate aerobes or facultative anaerobes (35,36).

Tuberculous abscesses typically have high lipid, lactate peaks and no peaks for amino acids (leucine, isoleucine, and valine) at 0.9 ppm, succinate at 2.41 ppm, acetate at 1.92 ppm, and alanine at 1.48 ppm, in contrast to the pyogenic ones, which have peaks for all these metabolites.

DWI

A markedly reduced ADC is the typical feature of abscesses; in fact, neoplasm more often have a facilitated diffusion while abscesses more probably have a restricted one in their necrotic portion, albeit some reports showed overlapping features (37).

Perfusion imaging

The typical feature is low rTBV; as a matter of fact, high-grade primary neoplasms and metastases can be differentiated from brain abscesses with perfusion MR imaging, in which the wall of necrotic or cystic neoplasms tends to have higher rTBV compared with the capsule of an abscess (37).

Encephalitis

MRS

The typical characteristics are elevated peaks of lactate, choline, and myoinositol and reduced NAA signal. Encephalitis tend to mimic low-grade gliomas, with reduction of the NAA signal and elevation of the choline and myoinositol peaks.

There is gradual normalization of the MR spectrum in about 1 year after the acute phase of encephalitis (38).

DWI

The typical DWI feature for encephalitis is variable ADC. Encephalitis typically has low ADC values although this finding is less consistent than in infarcted tissue. DWI may also shed light on the severity of the process, because fulminant cases more probably cause restricted diffusion (38).

Perfusion imaging

It is not known a typical perfusion imaging feature: a case report of perfusion computed tomography tends to favor an elevated perfusion in the acute phase (39).

Al-Okaili *et al.* (40) also investigated the role of commonly used advanced imaging techniques in the differentiation among intracranial masses in adults and suggested a practical MRI-based algorithm including results from post-contrast MRI, diffusion-weighted MRI, perfusion MRI, and 1H MRSI to improve the diagnosis and classification of these lesions.

They identified 44 patients with high-grade and 14 with low-grade primary neoplasms, 24 with abscesses, 12 with lymphoma, 11 with TDLs, 5 with metastases, and one with encephalitis, all histologically-confirmed, who had undergone conventional (transverse and sagittal T1-weighted spin-echo, transverse T2-weighted fast spin-echo, transverse fast fluid attenuated inversion recovery and contrast-enhanced transverse and coronal T1-weighted spin-echo) and advanced MR imaging; all images where acquired with a 1.5 T system. However, only 40 patients (25 women, 15 men; mean age, 45 years) had undergone all studies and had data to permit the completion of the entire strategy.

The accuracy, sensitivity, and specificity of the strategy, respectively, were 90%, 97%, and 67% for discrimination of neoplastic from nonneoplastic diseases, 90%, 88%, and 100% for discrimination of high-grade from low-grade neoplasms, and 85%, 84%, and 87% for discrimination of high-grade neoplasms and lymphoma from low-grade neoplasms and nonneoplastic diseases.

The reported sensitivity of conventional MR imaging is lower than the sensitivity of this strategy (88%) (22,27). The performance of perfusion MR imaging alone also appeared to be lower.

These results suggest that integration of advanced imaging techniques with conventional MRI may help to improve the reliability of the diagnosis and classification of brain lesions.

Advanced MRI in glioma grading

Diagnosing tumor type and grade non-invasively have an important influence on management decisions and prognosis; in fact, high-grade brain tumors are usually treated more aggressively than low-grade tumors and for this reason preoperative diagnosis of tumor grade is very important.

According to the WHO classification gliomas are divided into 4 grades (I–IV); this classification is based on specific histologic features: cellularity, nuclear atypia, mitotic activity, pleomorphism, vascular hyperplasia, and necrosis. Grade I glioma is a single group composed of gliomas with a relative benign biology and indolent clinical course (pilocytic astrocytoma, pleomorphic xanthoastrocytoma, subependymal giant cell astrocytoma). The remaining diffuse gliomas are divided in to grades II–IV (41).

Many important information in the characterization of tumor aggressiveness and grade such as

the contrast material enhancement, perienhancement edema, distant tumor foci, hemorrhage, necrosis, mass effect may be provided by cMRI although sometimes this technique has shown to be unreliable with a sensitivity for glioma grading ranging from 55.1% to 83.3% (25,41).

The incorporation of physiologic data provided by the advanced MRI techniques has given to neuroradiologists the opportunity to combine biology with radiology in brain tumors and so to obtain clinically relevant informations for the assessment of malignancy (41).

In a wide variety of tumors, it has been histologically verified an inverse correlation between minimum ADC (ADCmin) and tumor cellularity (42).

Due to substantial overlap in ADC values among different grades of glioma, the role of DWI in the preoperative assessment of glioma grade is clinically insignificant and remains investigational, although some reports have shown that ADCmin values below a cutoff in the range of 1.7 to 2.5 may be useful in differentiating low from high grade gliomas (43); this is caused by the heterogeneity of gliomas across different grades, within the same grade, and even within a single given tumor. In fact, a given glioma, usually of high grade, often contains a continuum of histologic features of grades II–IV and the site of tumor biopsy or resection is an important factor in the process of tumor grading being subject to sampling error or undersampling.

Actually, the role of MRS in glioma grading in the clinical preoperative setting, has not been proved enough accurate to replace tissue diagnosis and grading (41).

Although MRS seems to be unreliable in the definition of tumor differential diagnosis, the presence of high choline/NAA peak height ratios has been demonstrated in a number of studies to be predictive of the presence of high-grade tumor (44,45). In the same way, a lipid/lactate peak in untreated glioma suggests the presence of necrotic grade IV tumor (44,46).

In fact, the regions of lactate most probably represent areas of hypoxic but viable tumor, whereas the regions of mobile lipid represent necrotic non-viable tissue.

MRS has shown to be a useful tool to increase the accuracy of tumor biopsy by targeting areas of metabolically active tumor, corresponding to areas with high choline/NAA ratios, within areas of heterogeneous glioma and thus reducing the false-negative rate (47).

The degree of tumor angiogenesis and capillary permeability, which are important biologic markers of malignancy, grading, and prognosis, particularly in gliomas (41), are measurable targets of perfusion MRI. Some reports have widely shown the strong correlation between the maximum rCBV measured in a tumor and the histologic tumor grade in documented or suspected astrocytoma (48-50). In fact, as noticed above, a tumor with an rCBV similar to or greater than cortex should strongly favor the presence of IV grade tumor.

A maximum rCBV value has proved its utility in preoperative planning to ensure biopsy, resection, or ablation of the highest-grade portion of a heterogeneous tumor despite of some limitations such as low spatial resolution, susceptibility artifact, quantitation, and the difficulty of making longitudinal comparisons between echoplanar datasets (51,52).

It has also been proved the robustness of the correlation of increased permeability with increasing tumor grade (53-55).

It is not surprising to find that permeability measures are slightly less predictive of tumor grade than rCBV (55,56) since, as well as neoangiogenesis, there is a large number of physiologic processes that may increase capillary permeability.

Albeit permeability is independent of blood volume (57), its measures are strongly correlated with rCBV in high grade glioma (58), probably because of the coregulation of neoangiogenesis and increased vascular permeability by VEGF and other proangiogenic factors.

The role of MRS and perfusion in glioma grading compared with cMRI was investigated by Law *et al.* (22), who retrospectively evaluated 160 patients that underwent

some preoperative MR examinations [cMRI, multivoxel 2D proton chemical shift imaging (CSI), dynamic contrast agent-enhanced T2*-weighted gradient echo, echo-planar imaging] and had histopathologic results for comparison; patients age ranged from 4 to 82 years, with a mean of 43 years (108 male and 52 female patients).

A modified Ringertz's three-tier classification of gliomas was used for the histopathologic evaluation: grade 1, low-grade glioma; grade 2, anaplastic glioma; and grade 3, glioblastoma (GBM) multiforme. The imaging classification was divided into two tiers. Anaplastic gliomas and GBM multiforme were considered high-grade gliomas, and this group comprised 120 patients. The low-grade gliomas group comprised 40 patients (22).

For rCBV and metabolite ratios, it was used a receiver operating characteristic (ROC) curve analyses to evaluate the performance of simple diagnostic tests that declared a glioma to be high grade and permitted a determination of the sensitivity, specificity, PPV, NPV, and total error associated with each measure. To determine the potentially useful values for rCBV, Cho/Cr, and Cho/NAA in differentiating low- from high-grade gliomas, they found some thresholds that minimized the observed number of tumor grade misclassifications (C2 error = fraction of misclassified tumors) and maximized the average of the observed sensitivity and specificity (C1 error). Hence, C1 = 1 – (sensitivity + specificity)/2.

The sensitivity, specificity, PPV, and NPV for determining a high-grade glioma with conventional MR imaging were 72.5%, 65.0%, 86.1%, and 44.1%, respectively. The statistical analysis demonstrated that a threshold value of 1.75 for rCBV provided a sensitivity, specificity, PPV, and NPV of 95.0%, 57.5%, 87.0%, and 79.3%, respectively. A threshold values of 1.08 and 1.56 for Cho/Cr and 0.75 and 1.60 for Cho/NAA provided the minimum C2 and C1 errors, respectively, for determining high-grade glioma. The combination of rCBV, Cho/Cr, and Cho/NAA resulted in a sensitivity, specificity, PPV, and NPV of 93.3%, 60.0%, 87.5%, and 75.0%, respectively.

Some significant differences were noted in the rCBV and Cho/Cr, Cho/NAA, and NAA/Cr ratios between low- and high-grade gliomas ($P<0.0001$, 0.0121, 0.001, and 0.0038, respectively).

There was no statistically significant difference in the rCBV, Cho/Cr, Cho/NAA, and Cho/Cr ratios between the anaplastic gliomas and GBM multiforme.

The rCBV measurements and metabolite ratios both individually and in combination can increase the sensitivity and PPV when they are compared with conventional MR imaging alone in determining glioma grade.

The lower sensitivity and specificity of Cho compared with rCBV suggests that although Cho levels may correlate directly with tumor cellularity, tumor cellularity may not correlate directly with tumor grade. The tumor grade seems to correlate more likely with necrosis, nuclear atypia, mitoses, and vascular hyperplasia; hence, rCBV may provide stronger correlation with tumor grade than Cho does. This study demonstrates that rCBV and metabolite measurements can improve preoperative tumor grading. MRS and perfusion MR imaging are useful adjuncts to cMRI in planning postoperative chemotherapy, antiangiogenic therapy, and radiation therapy. Since these techniques avoid some of the problems of sampling error associated with histopathologic examination, it is conceivable that such methods may provide a more accurate overall assessment of tumors (41).

Advanced MRI in preoperative planning

Malignant brain tumors such as GBM multiforme often invade the surrounding tissue and WM tracts, having an infiltrative pattern of growth; in fact, the tumor can extend microscopically for several centimeters past the radiographically detected margin of disease (59). Furthermore, infiltrative brain tumors are surrounded by extensive areas of edema, as detected on T2-weighted imaging.

There is not a clear transition between the tumor edge and peritumoral edema: in metastatic tumors, this peritumoral edema is thought to consist of pure water, while in infiltrative tumors it has often been shown to contain tumor cells that have spread into the edematous tissue.

Conventional MR imaging is not able to detect this minute cellular infiltration and to describe the relationship between tumor and neighboring WM tracts (*Figure 3*); some studies have shown the presence of tumor cells beyond tumor borders as defined by these modalities; this fact represents a serious challenge for treatment planning, a problem that can lead to suboptimal treatment, postoperative neurological deficits and a worse prognosis (60). In successful surgical resection, the neurosurgeon must excise the tumor with the greatest extent possible while minimizing injury to nearby healthy tissue.

DTI is a promising tool to evaluate the peritumoral region in patients with intracranial brain tumors due to the microstructural information that this technique can provide.

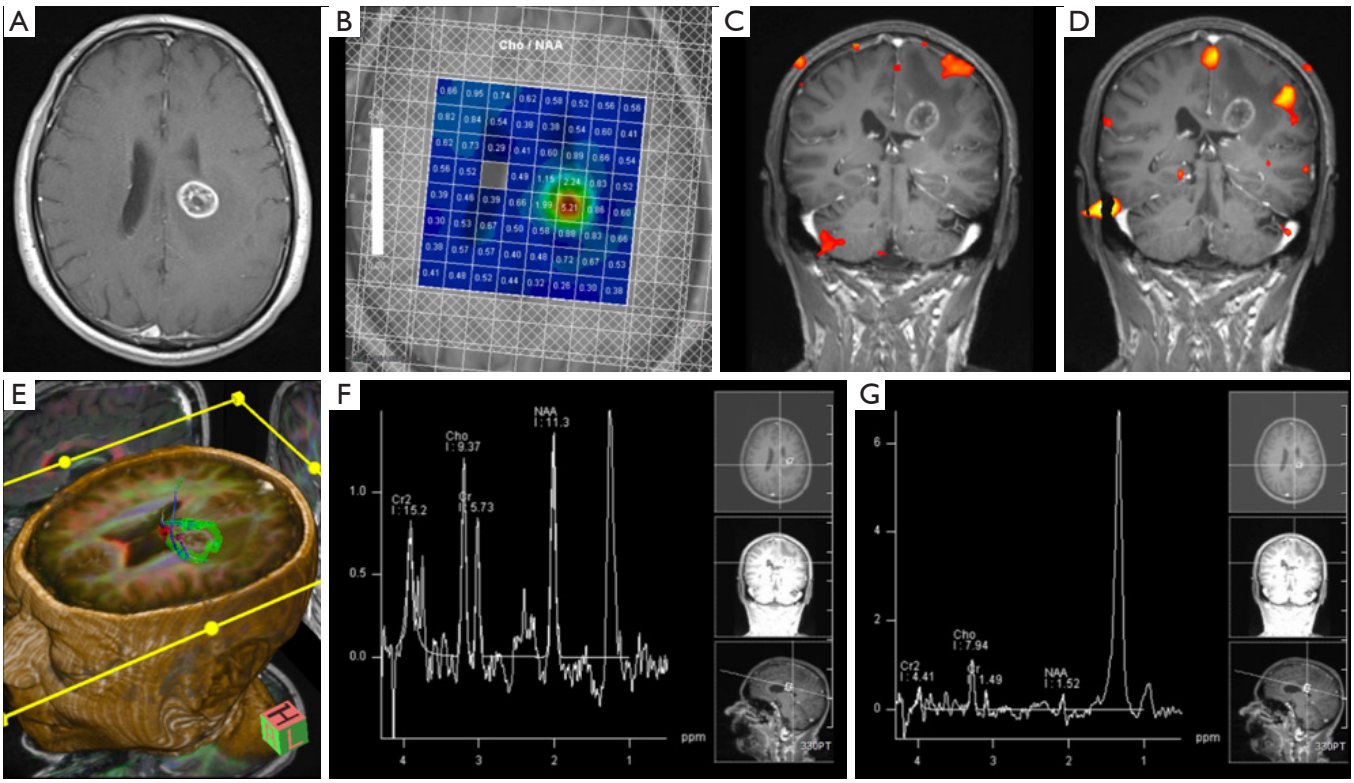

Figure 3 Left frontal lobe GBM: (A) axial T1 post gadolinium administration; (B) axial multi-voxel MRS color-coded map of choline/NAA; (C) coronal BOLD showing motor activation; (D) coronal BOLD showing speech activation; (E) DTI with particular of fibres bundles close to the lesion; (F,G) spectra from a single voxel within the GBM. GBM, glioblastoma; MRS, magnetic resonance spectroscopy; NAA, n-acetylaspartate; DTI, diffusion-tensor imaging.

It has been demonstrated a diffusion alteration within this surrounding edema in both high-grade gliomas and metastatic tumors compared with internal controls, reflecting the presence of, at minimum, increased extracellular water.

It has been demonstrated further, by using DWI, that the diffusivity of the peritumoral edema varies

in direct proportion to the grade of the tumor it encompasses: high-grade gliomas are associated with edema of high trace value [mean diffusivity (MD)], whereas the low-grade gliomas or nonglial tumors are associated with a low trace one, as it has been indicated by Morita *et al.* (61). They concluded that the "higher diffusivity of water molecules within the area of edema associated with high-grade gliomas is likely to reflect destruction of the extracellular matrix ultrastructure by malignant cell infiltration" (61).

A current work demonstrates that, compared with normal-appearing WM, there is an increase in MD and a decrease in FA measurements in the surrounding tissue of both primary and metastatic brain tumors: in fact, it is known that the bigger is the quantity of free water in the tissue, the greater will be the magnitude of diffusion (increased MD) and the more disorganized it will become (decreased FA) (62).

Lu *et al.* (63) found that, comparing the peritumoral region of metastatic lesions and glioma, the peritumoral MD was higher in the former than in the latter while it has been demonstrated no difference in the peritumoral FA between the two tumor types.

Hence, we can infer that the reduced FA surrounding gliomas may be correlated not only to increased extracellular water but also to axonal disorganization caused by infiltration of the tumor beyond its detectable margin.

The FA values were measured by Sundgren *et al.* (64) in the normal-appearing WM bordering the peritumoral edema of recurrent and nonrecurrent tumors, resulting in a significantly lower FA values in the normal tissue

that encompasses recurrent tumors compared with non-recurrent ones. This evidence suggests the presence of cellular micro infiltration into the peritumoral WM in recurrent tumors.

This hypothesis is in tight accordance with the known correlation between tumors of high infiltrative capacity and the associated recurrence risk.

Earlier studies have demonstrated that the occult infiltration by aggressive cancer that causes subtle WM disruption may be detected by DTI metric changes (65).

In another study in 2004, Lu *et al.* (66) tried to define if trough the MD and FA it was possible to discriminate between intra-axial from extra-axial lesions, metastatic lesions from gliomas, and high-grade (World Health Organization grades III–IV) from low-grade (World Health Organization grade II) gliomas studying retrospectively the DTI data from 40 patients.

The investigators, to define properly the extent of tissue infiltration, used a third parameter that they termed the "tumor infiltration index (TII)", which was calculated from DTI data by the following formula:

$$\mathrm{TII} = \left(FA\exp - FAobs\right)\times 103 \quad [2]$$

where *FAexp* is the expected FA for the corresponding MD, assuming no tumor infiltration (as determined by a linear regression analysis of such data) and *FAobs* is the currently measured FA.

In the purpose of making the results coherent with those of the study above, the TII of non-infiltrative tumors should be approximately zero, while the TII of infiltrative tumors should be considerably higher. Finally, they indeed achieved this outcome: in fact gliomas had a mean TII of 64, while metastases and meningiomas had a mean TII of 0.

The efficacy of DTI in differentiating normal and tumor infiltrated peritumoral tissue was further shown by Provenzale *et al.* (67). They found, comparing the mean FA values in peritumoral hyperintense regions with those of normal WM, a ratio of 43% for glioma and 65% for meningioma (P=0.05), while the mean FA values for normal-appearing WM surrounding the tumors were 83% of the normal value for patients with gliomas and 100% for those with meningiomas (P=0.01).

In other words, even though the difference in FA in the hyperintense regions of gliomas and meningiomas was evident, it was statistically insignificant; however, the decrease in FA in the normal-appearing encompassing WM was significant, being the decrement greater in patients with glioma (P=0.01).

This result shows that DTI may have the potential to detect tumoral infiltration that cannot be discerned by cMRI techniques, revealing a disparity in the FA of peritumoral normal-appearing tissue and that this disparity is greater in the tissue neighboring gliomas rather than meningiomas.

Fractional anisotropy was correlated with the distance from visible tumor margins in gliomas by Deng *et al.* (68), who found that the value increases in direct proportion to the distance from the tumor.

Moreover, they obtained some tissue samples from the regions of interest as determined on MR imaging and finally observed a negative association between FA values from the peritumoral edema of gliomas and the degree of tumor infiltration (categorized as mild, moderate, severe, or no infiltration) (68).

These results, which are coherent with the past findings, show that a reduction in FA in the peritumoral region, compared with the corresponding contralateral one, is a marker of tumor invasion past the tumor borders, as detected on T2-weighted images and could be used as a quantitative index of tumor cell infiltration.

Although the tissue architecture can be highly variable and therefore provide inconsistent or nonspecific results, the use of adjunctive DTI metrics can improve the quality of findings and facilitate accurate and specific conclusions.

A recent study of Farshidfar *et al.* (69) evaluated the application of DTT imaging in the presurgical assessment of gliomas, introducing this new modality and its importance to physicians and imaging centers.

Ten patients (mean age: 48.6, ranging from 36 to 60 years old) with intra-axial brain tumor (verified by conventional MRI) and suspicion of glioma underwent conventional brain MRI pulse sequences (T1-weighted images 3D fast spoiled gradient recalled echo sequences were acquired to overlay the selected fibers on them; T2-weighted images were acquired before fiber tracking for a better evaluation of tumor margins if necessary) and DTT imaging between December 2011 and February 2013 with a 1.5 Tesla system using 64 independent diffusion encoding directions. All acquired images (FA, ADC maps, color- FA and 3D reconstructed fibers) were evaluated by an expert radiologist to report which neuronal fibers were affected by the tumor and in which way. They categorized the type of involvement of WM tracts into four groups according to Witwer *et al.*'s criteria—(I) displaced (deviated) WM tracts: if they maintained normal anisotropy relative to the corresponding tract in the contralateral hemisphere but were situated in an abnormal location or with an

abnormal orientation on color-coded orientation maps; (II) edematous: if they maintained normal anisotropy and orientation but demonstrated high signal intensity on T2-weighted MR images; (III) infiltrated: if they showed reduced anisotropy but remained identifiable on orientation maps; (IV) disrupted (destroyed): if anisotropy was markedly reduced such that the tract could not be identified on orientation maps.

The results with fiber tracking images were then shown to the neurosurgeons and the treatment procedures before and after fiber tracking were recorded. In seven patients (4 of them with deviation or compression and no destruction and infiltration of WM near tumor, 3 of them with infiltration or displacement or destruction of WM adjacent), the treatment technique changed from radiotherapy to craniotomy, which is more effective to improve prognosis. In another patient, physicians preferred to avoid surgery because of many connections between tumor and adjacent WM tracts; the operation strategy before tractography in this patient was craniotomy.

In one patient, the corticospinal tract went through the tumor, so the treatment plan (radiotherapy) did not change.

In one patient with deviation and compression of WM tracts near tumor, the operation strategy changed from radiosurgery to craniotomy.

According to DTT results, there was a change in the treatment in approximately all patients, and in one of them helped to plan a treatment procedure with more assurance. There were no significant additional neurological deficits after surgery, except in one patient who was temporarily hemiplegic for one week.

As we can infer from this work, the informations provided by the tractography are useful to eventually change the treatment strategy and to plan more accurately the treatment technique leading to fewer postoperative neurological deficits and better outcomes.

Advanced MRI in the therapeutic response

It is increasingly important to be able to predict tumor progression at earlier stages, when patients keep a performance status such that they can tolerate further therapies, because of the availability of improving second- and third-line treatments (70,71); it is also critical to accurately assess which gliomas on follow-up imaging are progressing on a current treatment regimen so that therapy can be modified appropriately.

According to the Macdonald criteria [the response criteria of supratentorial malignant gliomas published in 1990 (72)], the enhancing tumor area was the primary feature used in the radiologic assessment of tumor response and disease progression and cMRI was the best tool to detect early treatment-related changes. However, given that standard therapy for high grade glial tumors usually includes radiation as well as TMZ (73), early tumor progression can be simulated by changes in contrast enhancement detected with cMRI after or during treatment. In fact, various non-tumorous processes, such as treatment- related inflammation, postsurgical changes, ischemia, subacute radiation effects, and radiation necrosis, may induce increased enhancement (74).

Relatively recently, it was observed the occurrence of progressive MRI lesions immediately after the end of concurrent chemotherapy and radiation therapy (CCRT) with temozolomide (TMZ), with spontaneous improvement with no further treatments and this is related to pseudoprogression, for which rates were reported to be 20–30% (75-77).

Nevertheless, due to the absence of established differentiating features in conventional contrast-enhanced MR imaging (74), there was a revision of the Response Assessment in Neuro-Oncology (or RANO) criteria for high-grade gliomas such that, within the first 12 weeks after completion of radiation therapy, when pseudoprogression is most prevalent, progression can be determined only if the most of the new enhancement is outside the radiation field or if there is pathologic confirmation of progressive disease (78).

Considering that cytotoxic radiation and chemotherapy reduce tumor cellularity, increasing ADC within a given area of tumor (79,80), DWI may be a useful tool to following tumor treatment response and subsequent recurrence (*Figure 4*).

Gupta *et al.* (81) hypothesized that diffusion restriction, when present outside of the confines of enhancing tumor, may be a good predictor of tumor progression.

In their research, they reviewed the brain MR imaging scans (including DWI and ADC maps) of 208 patients with GBM. Sixty-seven of 208 patients (32%) with restricted diffusion in or adjacent to the tumor were identified and the study cohort was formed by 27 patients (20 man and 7 women; median age 53, range: 34–74 years) with low-ADC lesions and no corresponding enhancement.

If a patient developed new enhancement concordant with the low-ADC lesion, all available advanced imaging (DSC T2* MR perfusion, DCE T1 MR perfusion, 3D multivoxel

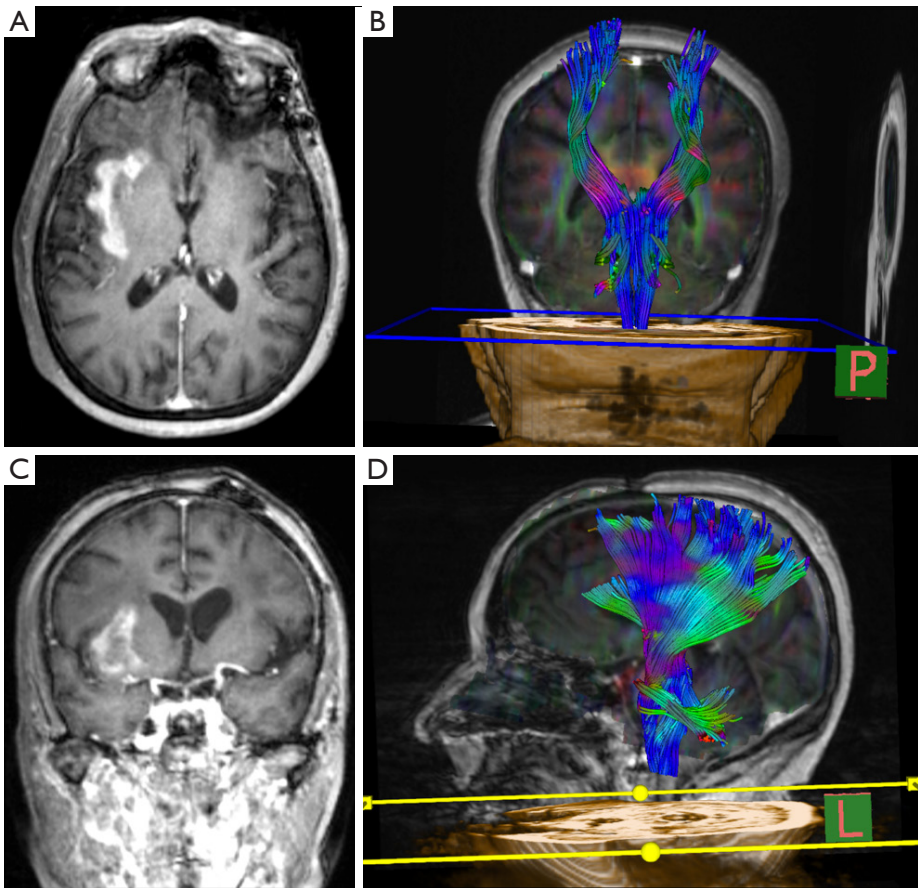

Figure 4 Right frontal lobe GBM recurrence after surgery: (A) axial and (C) coronal T1 post gadolinium administration; (B) coronal and (D) sagittal DTI representing the spinothalamic tract. GBM, glioblastoma; DTI, diffusion-tensor imaging.

PROBE CSI MRS) was reviewed by a board-certified neuroradiologist to determine the etiology of that new enhancement.

An aMRI result was considered as representing tumor if the following criteria, commonly applied in the literature, were satisfied: rCBV =1.75 (on DSC MR perfusion), maximal bolus wash-in slope >2 {on DCE MR perfusion [140]} or Cho/NAA >2.2 (MRS) (17,82,83).

The investigators used the Wilcoxon signed rank test, competing risk analysis, and Kaplan-Meier curves to compare the mean drop in ADC values, assess enhancement-free survival, and determine overall survival, respectively.

Twenty-three (85.2%) patients developed gadolinium-enhancing tumor at the site of restricted diffusion a median of 3.0 months later (95% CI, 2.6–4.1 months). The mean decrease in ADC was 22.9% from baseline (P=0.001). The 3-month enhancement-free survival probability was 0.481 (95% CI, 0.288–0.675). The 12-month overall survival probability was 0.521 (95% CI, 0.345–0.788).

This research has proved that, despite of antiangiogenic therapy with bevacizumab, the occurrence of isolated low-ADC lesions in a subset of patients with GBM anticipate and so may predict the development of concordant enhancing lesions at the same site.

Chu *et al.* (84) have investigated the role of histogram analysis of ADC maps obtained at standard- and high-b-value (1,000 and 3,000 sec/mm^2, respectively) in the differentiation of true progression from pseudoprogression in GBM treated with radiation therapy and concomitant TMZ.

In this retrospective study thirty patients (16 men, 14 women; mean age 50.8 years; age range, 25–72 years) with histopathologically proved GBM, who had undergone CCRT with TMZ, underwent 3T DWI with b values of 1,000 and 3,000 sec/mm^2 and corresponding ADC

maps were calculated from entire newly developed or enlarged enhancing lesions after completion of CHRT. The investigators compared the histogram parameters of each ADC map between true progression (n=15) and pseudoprogression (n=15) groups by using the unpaired Student t-test and then they used the ROC curve analysis to determine the best cutoff values for predictors in the differentiation of true progression from pseudoprogression; finally the best cutoff value was used to validate the results in an independent test set of nine patients.

In terms of cumulative histograms, the fifth percentile of both ADC at b value of 1,000 sec/mm^2 (ADC1000) and the ADC at b value of 3,000 sec/ mm^2 (ADC3000) were significantly lower in the true progression group than in the pseudoprogression one (P=0.049 and P=0.001, respectively).

In contrast, there was no significant difference between both the mean ADC1000 and the mean ADC3000 in the two groups.

Comparing the diagnostic values of the parameters derived from ADC1000 and ADC3000, it was found a significant difference (0.224, P=0.016) between the area under the ROC curve of the fifth percentile for ADC1000 and that for ADC3000 (0.757 and 0.981, respectively).

The measure of a fifth percentile value lower than 929×10^6 mm^2/sec for ADC1000 or lower than 645×10^6 mm^2/sec for ADC3000 allowed to diagnose the true progression for newly developed or enlarged enhancing lesions inside the radiation field after ChRT with TMZ.

The sensitivity and specificity of ADC1000 were 73.3% (11 of 15 patients) and 73.3% (11 of 15 patients), respectively; the sensitivity and specificity of ADC3000 were 93.3% (14 of 15 patients) and 100% (15 of 15 patients), respectively.

The confirmation came from the results of the independent test set (9 patients) enabling us to consider the fifth percentile of the cumulative ADC histogram obtained at high b value as the most promising parameter for the differentiation of true progression from pseudoprogression showing a sensitivity, specificity, and overall accuracy of 75% (three of four patients), 100% (five of five patients), and 88.9% (eight of nine patients), respectively, being the results similar to those of the retrospective study.

The accuracies were 66.7% (six of nine patients) and 88.9% (eight of nine patients) based on the fifth percentile of both ADC1000 and ADC3000 in the independent test set, respectively.

Some investigators applied the MRS to discriminate between radiation-induced tissue injury and tumor recurrence in adult and pediatric brain tumor patient post-radiation, after gamma knife radiosurgery, and brachytherapy. The increase of Cho signals (evaluated as Cho levels relative to Cho signal in normal-appearing tissue, Cho/Cr or Cho/NAA ratios) suggested the recurrence, while a significant reduction of Cho (and Cr) levels favored the radiation necrosis (85).

Necrotic regions may also show elevated lipid and lactate signals (47,86,87).

In a recent MRSI work, 31 patients with a previous diagnosis of an intracranial tumor were retrospectively studied to differentiate between recurrent tumor and radiation necrosis, reporting a sensitivity of 85%, a specificity of 69% using the Cho/NAA ratio (88).

Although MRSI achieved a good separation between pure necrosis and pure tumor, the comparison with biopsy specimens indicated that this technique cannot reliably differentiate the tissue containing mixed tumor/ radiation necrosis from tumor or radiation necrosis (86).

With the addition of ADC values to MRSI parameters there was an improvement in the differentiation between pure tumor and radiation necrosis (which exhibits higher ADC values than tumors) but not between mixed tissue and pure tumor or pure necrosis (89,90). The diagnostic accuracy of MRS in the discrimination of radiation necrosis may be improved if spectra of both the abnormal and normal tissue are available pre- and post-treatment (87).

In a cohort of 27 patients with gliomas grade (I–IV) treated with a combination of surgery, chemotherapy and radiation therapy MRS has proved to be able to differentiate patients with stable disease and with disease progression.

The investigators examined the patient at least twice, with a lapse of time between studies of 8.3±5.1 and of 49±41 months after the beginning of disease. In patient with stable disease the normalized Cho intensity changes were smaller than a critical value of 35% (range, 33% to 28%), while in the progressive disease the changes in normalized Cho between studies were larger than 45% (range, 46% to 104%). It was also demonstrated a very good agreement with survival data (16).

MRSI has also been used to predict the onset of new contrast enhancement on cMRI after therapy.

In a prospective clinical trial that included patients with GBM, the investigators put in relation the locations of MRSI abnormality at baseline with a new contrast enhancement and abnormal MRSI area after treatment with radiation and chemotherapy (91). At relapse, 82% of the 17 voxels with Cho/NAA ≥2 at baseline showed either

continuing or new contrast enhancement (as compared to 15% of 323 voxels with normal Cho/NAA ratio).

The combination of MRSI and postcontrast T1 and T2-weighted MRI may better predict regions of relapse after treatment than cMRI alone (91).

Perfusion MR has shown to be a very promising tool in the evaluation of treatment response in brain tumors.

Yun *et al*. (92) have explored the role of dynamic contrast material-enhanced MRI in the differentiation of true progression from pseudoprogression in patients with GBM on the basis of findings in entirely newly developed or enlarged enhancing lesions after concurrent radiation therapy and chemotherapy with TMZ; they have also evaluated the diagnostic performance of quantitative pharmacokinetic parameters such as the volume transfer constant (Ktrans), the extravascular extracellular space per unit volume of tissue(ve), and the blood plasma volume per unit volume of tissue (vp).

In this prospective study were included thirty-three patients with histopathologically proven GBM, who had undergone concurrent radiation therapy and chemotherapy (22 men and 11 women; age range, 28–82 years) and were confirmed to have true progression [n=17 (52%)] or pseudoprogression [n=16 (48%)] after the end of adjuvant TMZ according to the RANO criteria.

Conventional MRI (transverse and coronal T1- weighted imaging performed before and after contrast enhancement, transverse fluid-attenuated inversion recovery sequence and T2-weighted imaging) and dynamic contrast-enhanced MR (by using a 3.0-T imaging unit with a 32-channel head coil) were performed and then they calculated the imaging-derived pharmacokinetic parameters, including Ktrans, ve, and vp, for newly developed or enlarged enhancing lesions.

Finally, the investigators used the unpaired *t*-tests and then multivariable analysis to compare these parameters between the true progression (n=17) and pseudoprogression (n=16) groups.

The mean Ktrans and ve were higher in the true progression group than in the pseudoprogression one (mean Ktrans ± standard deviation: 0.44±0.25 and 0.23±0.10 min^{-1} for true progression and pseudoprogression groups, respectively, P=0.004; and mean ve, 1.26±0.78 and 0.75±0.49 for true progression and pseudoprogression groups, respectively, P=0.034).

The 10th percentile value of Ktrans showed the highest AUC for distinguishing true progression from pseudoprogression. The AUCs, sensitivities, specificities, and positive and negative predictive values for mean Ktrans and the 10th percentile value were 0.756, 59%, 94%, 91%, and 68% and 0.801, 82%, 75%, 78%, and 80%, respectively. In addition, the 5th percentile value of ve has proved to have the highest AUC.

The AUCs, sensitivities, specificities, positive and negative predictive values for mean ve and the 5th percentile value were 0.750, 88%, 56%, 68%, and 82% and 0.813, 76%, 88%, 87%, and 78%, respectively. However, it was not noted a significant difference between the AUCs for the mean and 10th percentile Ktrans values or among the mean and 5th percentile ve values (P=0.05).

By means of the multivariable analysis it was noticed that mean Ktrans was the only independently differentiating variable (P=0.004) and that, using a threshold value of 0.347 min^{-1}, dynamic contrast-enhanced MR imaging had a sensitivity of 59% (10 of 17 true progressions) and a specificity of 94% (15 of 16 pseudoprogressions).

Thus, the overall accuracy of mean Ktrans was 76%, with correct classifications in 25 of the 33 patients.

As we can infer from these results, the pharmacokinetic parameters derived from perfusion MRI, including Ktrans and ve, may be objectively useful to differentiate true progression from pseudoprogression in the entire newly developed or enlarged enhancing lesion in patients with GBM after CHRT.

Bevacizumab is a humanized monoclonal antibody to the vascular endothelial growth factor (VEGF) A, who is actually used, for its antiangiogenic effect, in the setting of recurrent GBM (93).

Even though bevacizumab therapy frequently causes a rapid reduction in the enhancing-tumor component, a significative reduction of tumor mass occurs only in a fraction of patients because the radiologic response partly derives from the normalization of abnormally permeable vessels and not always from a true antitumor effect that would translate to a survival benefit (78,94,95).

Kickingereder *et al*. (96) explored the role of hemodynamic parameters derived from parametric response map (PMR) in patients with recurrent GBM who have received bevacizumab treatment to shed light on the effects of therapy on tumor blood flow and oxygenation status.

The cohort was formed by 71 patients who received a diagnosis of recurrent GBM and underwent conventional anatomic magnetic resonance imaging (T1-weighted pre- and post-contrast imaging) and dynamic susceptibility contrast material-enhanced MR imaging (T2-weighted gradient echo-planar sequence) with a 3T MR and a 12-channel headmatrix coil at baseline and at the first

follow-up examination after the initiation of bevacizumab therapy.

The investigators created a PMR with multistep (non-linear) registration of patient's post- to pretreatment images and voxel-wise subtraction between Gaussian-normalized relative cerebral blood volume (nrCBV) and Gaussian-normalized relative cerebral blood flow (nrCBF) maps. They stratified the voxels inside the tumor as being increased (PRM+) or decreased (PRM–) if they exceeded a threshold that represented the 95% confidence interval in the normal-appearing brain. The Cox proportional hazards models were used to establish a correlation with progression-free and overall survival.

A significant increase of the risks for disease progression and death occurred with (I) higher baseline nrCBV values [hazard ratio (HR) =1.86, P<0.01; HR =1.52, P<0.01] and nrCBF (HR =1.78, P<0.01; HR =1.86, P<0.01); and (II) higher PRM– of nrCBV (HR =1.03, P<0.01; HR =1.02, P<0.03) and nrCBF (HR =1.04, P<0.01; HR =1.03, P<0.01), but not with higher PRM+ of nrCBV and nrCBF and not for the relative change in mean nrCBV and nrCBF, confirming the superiority of the PRM approach. There was also an important growth of the magnitude of PRM– for both nrCBV and nrCBF for higher baseline values (P<0.01).

In this study, the voxel-wise PRM investigation of the hemodynamic alteration induced by bevacizumab therapy reveals that greater levels of PRM–, but not PRM+, increased the risk for disease progression and death in patients being treated for recurrent GBM.

There are two interpretations of the findings from PRM: according to parametric response, as expected from the mechanism of action of bevacizumab, PRM– indicate a stronger response to the therapy in tumors characterized by a high perfusion and then a higher degree of angiogenesis at baseline (97-99). The relative prognosis associated with tumors with a higher degree of angiogenesis at baseline does not change as a result of therapy; this is proved by the fact that PRM– is associated with decreased, rather than better survival, while there was no evidence that PRM+ is a treatment failure marker in terms of increased angiogenic potential of tumors despite the use of bevacizumab therapy.

In other words, tumors with a high degree of angiogenesis still retain this angiogenesis level despite a greater antiangiogenic effect of bevacizumab without a reversal of their biologic behavior and relative prognosis.

These findings suggest that these tumors exploit mechanisms that are different from the angiogenesis [i.e., progression without the need to satisfactorily reinitiate angiogenesis (proinvasive evasion)] or, regardless of a large decrease, the remaining comparatively high degree of angiogenesis is sufficient to keep them more aggressive (100).

This disclosure does not indicate that that bevacizumab therapy is ineffective, since, despite the fact that baseline parameters are predictive, bevacizumab still determines survival.

DCE-MRI parameters in tumor prognosis

GBM is the most frequent, most aggressive primary malignant brain tumor in adults (93) and necrosis has a central role in tumor aggressiveness (101). Necrosis is the strongest prognostic factor (as compared with other imaging characteristics) and is inversely correlated with patient survival (102).

Mitotic activity (103-105), microvascular density (103) and certain vascular patterns (104) are some of the prognosticators that have been identified within given histologic subtypes and tumor grades. Ki-67 (104) and the expression of VEGF (101), who are both proliferation markers, are also correlated to survival.

The microvascular environment is described by a certain number of parameters that derive from dynamic contrast-enhanced MR imaging (DCE-MR imaging) techniques.

The enhancing fraction (EnF) describes the proportion of perfused tumor tissue. CBV and CBF are commonly derived from dynamic susceptibility contrast techniques, while T1-weighted DCE-MR imaging generates the volume transfer coefficient (Ktrans), fractional volume of the extravascular extracellular space (ve), and fractional blood plasma volume (vp). In glioma, Ktrans, vp, EnF, CBV, and CBF have been shown to be in connection with the histologic grade and/or subtype of tumor (22,56,105).

In addition, Ktrans, EnF, and CBV are potentially grade-independent prognosticators (24,106,107).

The study of Mills *et al.* (108) has evaluated the relationships between these parameters and histologic features in GBM multiforme. Twenty-eight patients with newly presenting GBM multiforme underwent preoperative imaging (conventional imaging and T1 dynamic contrast-enhanced MRI). The investigators generated a parametric map of the initial area under the contrast agent concentration curve, contrast transfer coefficient, estimate of volume of the extravascular extracellular space, and estimate of blood plasma volume and calculated the EnF.

The assessment of subtype and the grading was performed using surgical specimens (World Health Organization classification system) and were characterized for necrosis, cell density, cellular atypia, mitotic activity, and overall vascularity scores. CD34 immunostaining was the method utilized to make the quantitative assessment of endothelial surface area, vascular surface area, and a vascular profile count. Then the relationships between MR imaging parameters and histopathologic features have been examined.

The presence of frank necrosis was associated with high values of contrast transfer coefficient (P=0.005); high values of the estimate of volume of the extravascular extracellular space were associated with a fibrillary histologic pattern (P=0.01) and with increased mitotic activity (P=0.05). Mitotic activity and histologic pattern were not correlated, suggesting that the correlation between the estimate of volume of the extravascular extracellular space and mitotic activity was independent of the histologic pattern.

Despite of the requirement of further work, including markers of proliferation and measures of VEGF expression, to establish the relationship between dynamic contrast-enhanced MRI parameters and more quantitative histologic measurements, this study indicates that the estimate of volume of the extravascular extracellular space is related to mitotic activity.

Conclusions

Advanced MRI is an essential tool in the study of brain tumors, integrating anatomics informations provided by cMRI with biologic and pathophysiological data of these tumors.

For this reason, although actually those informations are not already integrated into the existing histopathologic classification, aMRI constitute a mean through whom we could rationally tailor the therapy to each patient in order to maximize results, minimizing adverse effects (post-surgery neurological deficit, chemotherapy toxicity, etc.).

Although further studies are needed, especially with bigger cohorts of patients, aMRI showed that we can shed light on the prognosis and response to targeted chemotherapies.

On this purpose, some reports have evaluated imaging markers by direct comparison with molecular genotype and phenotype and patient outcome and this multidisciplinary approach seem to represent the future in the management of this pathologies.

Acknowledgments

Funding: None.

Footnote

Conflicts of Interest: All authors have completed the ICMJE uniform disclosure form (available at http://dx.doi.org/10.21037/jxym.2017.06.01). The authors have no conflicts of interest to declare.

Ethical Statement: The authors are accountable for all aspects of the work in ensuring that questions related to the accuracy or integrity of any part of the work are appropriately investigated and resolved.

References

1. Wen PY, Kesari S. Malignant gliomas in adults. N Engl J Med 2008;359:492-507.
2. Okada H, Kohanbash G, Zhu X, et al. Immunotherapeutic approaches for glioma. Crit Rev Immunol 2009;29:1-42.
3. Gruber ML, Buster WP. Temozolomide in combination with irinotecan for treatment of recurrent malignant glioma. Am J Clin Oncol 2004;27:33-8.
4. Young GS. Advanced MRI of Adult brain tumors. Neurol Clin 2007;25:947-73.
5. Hagmann P, Jonasson L, Maeder P, et al. Understanding diffusion MR imaging techniques: From scalar diffusion-weighted imaging to diffusion tensor imaging and beyond. Radiographics 2006;26:S205-23.
6. Stadlbauer A, Nimsky C, Buslei R, et al. Diffusion tensor imaging and optimized fiber tracking in glioma patients: Histopathologic evaluation of tumor-invaded white matter structures. Neuroimage 2007;34:949-56.
7. Ferda J, Kastner J, MukenSnabl P, et al. Diffusion tensor magnetic resonance imaging of glial brain tumors. Eur J Radiol 2010;74:428-36.

8. Mori S. editor. Introduction to Diffusion Tensor Imaging. Amsterdam: Elsevier, 2007.
9. Gui M, Peng H, Carew JD, et al. A tractography comparison between turboprop and spin-echo echo-planar Diffusion tensor imaging. Neuroimage 2008;42:1451-62.
10. Calvar JA. Accurate 1H tumor spectra quantification from acquisitions without water suppression. Magn Reson Imaging 2006;24:1271-9.
11. Moffett JR, Ross B, Arun P, et al. N-acetyl aspartate in the CNS: from neurodiagnostics to neurobiology. Prog Neurobiol 2007;81:89-131.
12. Wyss M, Kaddurah-Daouk R. Creatine and creatinine metabolism. Physiol Rev 2000;80:1107-213.
13. Essig M, Nguyen TB, Shiroishi MS, et al. Perfusion MRI: The Five Most Frequently Asked Clinical Questions. AJR Am J Roentgenol 2013;201:2214.
14. Omuro AM, Leite CC, Mokhtari K, et al. Pitfalls in the diagnosis of brain tumours. Lancet Neurol 2006;5:937-48.
15. Hourani R, Brant LJ, Rizk T, et al. Can proton MR spectroscopic and perfusion imaging differentiate between neoplastic and nonneoplastic brain lesions in adults? AJNR Am J Neuroradiol 2008;29:366-72.
16. Horská A, Barker PB. Imaging of Brain Tumors: MR Spectroscopy and Metabolic Imaging. Neuroimaging Clin N Am 2010;20:293-310.
17. Al-Okaili RN, Krejza J, Wang S, et al. Advanced MR Imaging Techniques in the Diagnosis of Intraaxial Brain Tumors in Adults. RadioGraphics 2006;26:S173-89.
18. Butzen J, Prost R, Chetty V, et al. Discrimination between neoplastic and nonneoplastic brain lesions by use of proton MR spectroscopy: the limits of accuracy with a logistic regression model. AJNR Am J Neuroradiol 2000;21:1213-9.
19. Howe FA, Barton SJ, Cudlip SA, et al. Metabolic profiles of human brain tumors using quantitative in vivo H-1 magnetic resonance spectroscopy. Magn Reson Med 2003;49:223-32.
20. Yang D, Korogi Y, Sugahara T, et al. Cerebral gliomas: prospective comparison of multivoxel 2D chemical-shift imaging proton MR spectroscopy, echoplanar perfusion and diffusion-weighted MRI. Neuroradiology 2002;44:656-66.
21. Lam WW, Poon WS, Metreweli C. Diffusion MR imaging in glioma: does it have any role in the preoperation determination of grading of glioma? Clin Radiol 2002;57:219-25.
22. Law M, Yang S, Wang H, et al. Glioma grading: sensitivity, specificity, and predictive values of perfusion MR imaging and proton MR spectroscopic imaging compared with conventional MR imaging. AJNR Am J Neuroradiol 2003;24:1989-98.
23. Smits M. Imaging of oligodendroglioma. Br J Radiol 2016;89:20150857.
24. Lev MH, Ozsunar Y, Henson JW, et al. Glial tumor grading and outcome prediction using dynamic spin-echo MR susceptibility mapping compared with conventional contrast-enhanced MR: confounding effect of elevated rCBV of oligodendrogliomas. AJNR Am J Neuroradiol 2004;25:214-21.
25. Möller-Hartmann W, Herminghaus S, Krings T, et al. Clinical application of proton magnetic resonance spectroscopy in the diagnosis of intracranial mass lesions. Neuroradiology 2002;44:371-81.
26. Burtscher IM, Skagerberg G, Geijer B, et al. Proton MR spectroscopy and preoperative diagnostic accuracy: an evaluation of intracranial mass lesions characterized by stereotactic biopsy findings. AJNR Am J Neuroradiol 2000;21:84-93.
27. Law M, Cha S, Knopp EA, et al. High-grade gliomas and solitary metastases: differentiation by using perfusion and proton spectroscopic MR imaging. Radiology 2002;222:715-21.
28. Cha S, Knopp EA, Johnson G, et al. Intracranial mass lesions: dynamic contrast-enhanced susceptibility-weighted echoplanar perfusion MR imaging. Radiology 2002;223:11-29.
29. Chang L, Munsaka SM, Kraft-Terry S, et al. Magnetic Resonance Spectroscopy to Assess NeuroInflammation and Neuropathic Pain. J neuroimmune Pharmacol 2013;8:576-93.
30. Hartmann M, Heiland S, Harting I, et al. Distinguishing of primary cerebral lymphoma from highgrade glioma with perfusion-weighted magnetic resonance imaging. Neurosci Lett 2003;338:119-22.
31. Saindane AM, Cha S, Law M, et al. Proton MR spectroscopy of tumefactive demyelinating lesions. AJNR Am J Neuroradiol 2002;23:1378-86.
32. Bernarding J, Braun J, Koennecke HC. Diffusion and perfusion-weighted MR imaging in a patient with acute demyelinating encephalomyelitis (ADEM). J Magn Reson Imaging 2002;15:96-100.
33. Lai PH, Ho JT, Chen WL, et al. Brain abscess and necrotic brain tumor: discrimination with proton MR spectroscopy and diffusion-weighted imaging. AJNR Am J Neuroradiol 2002;23:1369-77.
34. Lai PH, Li KT, Hsu SS, et al. Pyogenic brain abscess:

findings from in vivo 1.5-T and 11.7-T in vitro proton MR spectroscopy. AJNR Am J Neuroradiol 2005;26:279-88.
35. Garg M, Gupta RK, Husain M, et al. Brain abscesses: etiologic categorization with in vivo proton MR spectroscopy. Radiology 2004;230:519-27.
36. Chang SC, Lai PH, Chen WL, et al. Diffusion weighted MRI features of brain abscess and cystic or necrotic brain tumors: comparison with conventional MRI. Clin Imaging 2002;26:227-36.
37. Chan JH, Tsui EY, Chau LF, et al. Discrimination of an infected brain tumor from a cerebral abscess by combined MR perfusion and diffusion imaging. Comput Med Imaging Graph 2002;26:19-23.
38. Sener RN. Rasmussen's encephalitis: proton MR spectroscopy and diffusion MR findings. J Neuroradiol 2000;27:179-84.
39. Nonaka M, Ariyoshi N, Shonai T, et al. CT perfusion abnormalities in a case of non-herpetic acute limbic encephalitis [in Japanese]. Rinsho Shinkeigaku 2004;44:537-40.
40. Al-Okaili RN, Krejza J, Woo JH, et al. Intraaxial Brain Masses: MR Imaging-based Diagnostic Strategy—Initial Experience. Radiology 2007;243:539-50.
41. Cha S. Update on Brain Tumor Imaging: From Anatomy to Physiology. AJNR Am J Neuroradiol 2006;27:475-87.
42. Hayashida Y, Hirai T, Morishita S, et al. Diffusion-weighted imaging of metastatic brain tumors: comparison with histologic type and tumor cellularity. AJNR Am J Neuroradiol 2006;27:1419-25.
43. Yu CS, Li KC, Xuan Y, et al. Diffusion tensor tractography in patients with cerebral tumors: a helpful technique for neurosurgical planning and postoperative assessment. Eur J Radiol 2005;56:197-204.
44. Catalaa I, Henry R, Dillon WP, et al. Perfusion, diffusion and spectroscopy values in newly diagnosed cerebral gliomas. NMR Biomed 2006;19:463-75.
45. Devos A, Lukas L, Suykens JA, et al. Classification of brain tumours using short echo time 1H MR spectra. J Magn Reson 2004;170:164-75.
46. Li X, Vigneron DB, Cha S, et al. Relationship of MR-derived lactate, mobile lipids, and relative blood volume for gliomas in vivo. AJNR Am J Neuroradiol 2005;26:760-9.
47. Gajewicz W, Grzelak P, Gorska-Chrzastek M, et al. The usefulness of fused MRI and SPECT images for the voxel positioning in proton magnetic resonance spectroscopy and planning the biopsy of brain tumors: presentation of the method [abstract]. Neurol Neurochir Pol 2006;40:284-90.
48. Maia AC, Malheiros SM, da Rocha AJ, et al. MR cerebral blood volume maps correlated with vascular endothelial growth factor expression and tumor grade in nonenhancing gliomas. AJNR Am J Neuroradiol 2005;26:777-83.
49. Shin JH, Lee HK, Kwun BD, et al. Using relative cerebral blood flow and volume to evaluate the histopathologic grade of cerebral gliomas: preliminary results. AJR Am J Roentgenol 2002;179:783-9.
50. Chaskis C, Stadnik T, Michotte A, et al. Prognostic value of perfusion-weighted imaging in brain glioma: a prospective study. Acta Neurochir (Wien) 2006;148:277-85.
51. Lupo JM, Cha S, Chang SM, et al. Dynamic susceptibility-weighted perfusion imaging of high-grade gliomas: characterization of spatial heterogeneity. AJNR Am J Neuroradiol 2005;26:1446-54.
52. Maia AC, Malheiros SM, da Rocha AJ, et al. Stereotactic biopsy guidance in adults with supratentorial nonenhancing gliomas: role of perfusion-weighted magnetic resonance imaging. J Neurosurg 2004;101:970-6.
53. Roberts HC, Roberts TP, Ley S, et al. Quantitative estimation of microvascular permeability in human brain tumors: correlation of dynamic Gd-DTPA-enhanced MR imaging with histopathologic grading. Acad Radiol 2002;9:S151-5.
54. Provenzale JM, Wang GR, Brenner T, et al. Comparison of permeability in high-grade and low-grade brain tumors using dynamic susceptibility contrast MR imaging. AJR Am J Roentgenol 2002;178:711-6.
55. Law M, Yang S, Babb JS, et al. Comparison of cerebral blood volume and vascular permeability from dynamic susceptibility contrast enhanced perfusion MR imaging with glioma grade. AJNR Am J Neuroradiol 2004;25:746-55.
56. Law M, Young R, Babb J, et al. Comparing perfusion metrics obtained from a single compartment versus pharmacokinetic modeling methods using dynamic susceptibility contrastenhanced perfusion MR imaging with glioma grade. AJNR Am J Neuroradiol 2006;27:1975-82.
57. Jackson A, Kassner A, Annesley-Williams D, et al. Abnormalities in the recirculation phase of contrast agent bolus passage in cerebral gliomas: comparison with relative blood volume and tumor grade. AJNR Am J Neuroradiol 2002;23:7-14.
58. Provenzale JM, York G, Moya MG, et al. Correlation of relative permeability and relative cerebral blood volume in high-grade cerebral neoplasms. AJR Am J Roentgenol 2006;187:1036-42.

59. Claes A, Idema AJ, Wesseling P. Diffuse glioma growth: a guerilla war. Acta Neuropathol 2007;114:443-58.
60. Sternberg EJ, Lipton ML, Burns J. Utility of Diffusion Tensor Imaging in Evaluation of the Peritumoral Region in Patients with Primary and Metastatic. AJNR Am J Neuroradiol 2014;35:439-44.
61. Morita K, Matsuzawa H, Fujii Y, et al. Diffusion tensor analysis of peritumoral edema using lambda chart analysis indicative of the heterogeneity of the microstructure within edema. J Neurosurg 2005;102:336-41.
62. Kimura T, Ohkubo M, Igarashi H, et al. Increase in glutamate as a sensitive indicator of extracellular matrix integrity in peritumoral edema: a 3.0-Tesla proton magnetic resonance spectroscopy study. J Neurosurg 2007;106:609-13.
63. Lu S, Ahn D, Johnson G, at al. Peritumoral diffusion tensor imaging of high grade gliomas and metastatic brain tumors. AJNR Am J Neuroradiol 2003;24:937-41.
64. Sundgren PC, Fan X, Weybright P, et al. Differentiation of recurrent brain tumor versus radiation injury using diffusion tensor imaging in patients with new contrast-enhancing lesions. Magn Reson Imaging 2006;24:1131-42.
65. Price SJ, Burnet NG, Donovan T, et al. Diffusion tensor imaging of brain tumours at 3T: a potential tool for assessing white matter tract invasion? Clin Radiol 2003;58:455-62.
66. Lu S, Ahn D, Johnson G, et al. Diffusion tensor MR imaging of intracranial neoplasia and associated peritumoral edema: introduction of the tumor infiltration index. Radiology 2004;232:221-8.
67. Provenzale JM, McGraw P, Mhatre P, et al. Peritumoral brain regions in gliomas and meningiomas: investigation with isotropic diffusion-weightedMRimaging and diffusion-tensorMRimaging. Radiology 2004;232:451-60.
68. Deng Z, Yan Y, Zhong D, et al. Quantitative analysis of glioma cell invasion by diffusion tensor imaging. J Clin Neurosci 2010;17:1530-6.
69. Farshidfar Z, Faeghi F, Mohseni M, et al. Diffusion Tensor Tractography in the Presurgical Assessment of Cerebral Gliomas. Neuroradiol J 2014;27:75-84.
70. Gutin PH, Iwamoto FM, Beal K, et al. Safety and efficacy of bevacizumab with hypofractionated stereotactic irradiation for recurrent malignant gliomas. Int J Radiat Oncol Biol Phys 2009;75:156-63.
71. Vredenburgh JJ, Desjardins A, Herndon JE 2nd, et al. Phase II trial of bevacizumab and irinotecan in recurrent malignant glioma. Clin Cancer Res 2007;13:1253-59.
72. Macdonald DR, Cascino TL, Schold SC Jr, at al. Response criteria for phase II studies of supratentorial malignant glioma. J Clin Oncol 1990;8:1277-80.
73. Stupp R, Mason WP, van den Bent MJ, et al. Radiotherapy plus concomitant and adjuvant temozolomide for glioblastoma. N Engl J Med 2005;352:987-96.
74. Ulmer S, Braga TA, Barker FG 2nd, at al. Clinical and radiographic features of peritumoral infarction following resection of glioblastoma. Neurology 2006;67:1668-70.
75. Taal W, Brandsma D, de Bruin HG, et al. Incidence of early pseudo-progression in a cohort of malignant glioma patients treated with chemoirradiation with temozolomide. Cancer 2008;113:405-10.
76. Brandsma D, Stalpers L, Taal W, et al. Clinical features, mechanisms, and management of pseudoprogression in malignant gliomas. Lancet Oncol 2008;9:453-61.
77. Chaskis C, Neyns B, Michotte A, et al. Pseudoprogression after radiotherapy with concurrent temozolomide for high-grade glioma: clinical observations and working recommendations. Surg Neurol 2009;72:423-8.
78. Wen PY, Macdonald DR, Reardon DA, et al. Updated response assessment criteria for high-grade gliomas: response assessment in neuro-oncology working group. J Clin Oncol 2010;28:1963-72.
79. Hein PA, Eskey CJ, Dunn JF, et al. Diffusion-weighted imaging in the follow-up of treated high-grade gliomas: tumor recurrence versus radiation injury. AJNR Am J Neuroradiol 2004;25:201-9.
80. Chan YL, Yeung DK, Leung SF, et al. Diffusion-weighted magnetic resonance imaging in radiation-induced cerebral necrosis. Apparent diffusion coefficient in lesion components. J Comput Assist Tomogr 2003;27:674-80.
81. Gupta A, Young RJ, Karimi S, et al. Isolated Diffusion Restriction Precedes the Development of Enhancing Tumor in a Subset of Patients with Glioblastoma. AJNR Am J Neuroradiol 2011;32:1301-6.
82. Law M, Oh S, Johnson G, et al. Perfusion magnetic resonance imaging predicts patient outcome as an adjunct to histopathology: a second reference standard in the surgical and nonsurgical treatment of low-grade gliomas. Neurosurgery 2006;58:1099-107; discussion 1099-107.
83. Young RJ, Knopp EA. Brain MRI: tumor evaluation. J Magn Reson Imaging 2006;24:709-24.
84. Chu HH, Choi SH, Ryoo I. Differentiation of True Progression from Pseudoprogression in Glioblastoma Treated with Radiation Therapy and Concomitant Temozolomide: Comparison Study of Standard and High-b-Value Diffusion-weighted Imaging. Radiology 2013;269:831-40.

85. Chernov MF, Hayashi M, Izawa M, et al. Multivoxel proton MRS for differentiation of radiation-induced necrosis and tumor recurrence after gamma knife radiosurgery for brain metastases. Brain Tumor Pathol 2006;23:19-27.
86. Rock JP, Hearshen D, Scarpace L, et al. Correlations between magnetic resonance spectroscopy and image-guided histopathology, with special attention to radiation necrosis. Neurosurgery 2002;51:912-9.
87. Law M. MR spectroscopy of brain tumors. Top Magn Reson Imaging 2004;15:291-313.
88. Smith EA, Carlos RC, Junck LR, et al. Developing a clinical decision model: MR spectroscopy to differentiate between recurrent tumor and radiation change in patients with new contrast-enhancing lesions. AJR Am J Roentgenol 2009;192:W45-52.
89. Rock JP, Scarpace L, Hearshen D, et al. Associations among magnetic resonance spectroscopy, apparent diffusion coefficients, and image-guided histopathology with special attention to radiation necrosis. Neurosurgery 2004;54:1111-7.
90. Zeng QS, Li CF, Liu H, et al. Distinction between recurrent glioma and radiation injury using magnetic resonance spectroscopy in combination with diffusion-weighted imaging. Int J Radiat Oncol Biol Phys 2007;68:151-8.
91. Laprie A, Catalaa I, Cassol E, et al. Proton magnetic resonance spectroscopic imaging in newly diagnosed glioblastoma: predictive value for the site of postradiotherapy relapse in a prospective longitudinal study. Int J Radiat Oncol Biol Phys 2008;70:773-81.
92. Yun TJ, Park CK, Kim TM, et al. Glioblastoma Treated with Concurrent Radiation Therapy and Temozolomide Chemotherapy: Differentiation of True Progression from Pseudoprogression with Quantitative Dynamic Contrast-enhanced MR Imaging. Radiology 2015;274:830-40.
93. Ostrom QT, Gittleman H, Liao P, et al. CBTRUS statistical report: primary brain and central nervous system tumors diagnosed in the United States in 2007-2011. Neuro-oncology 2014;16:iv1-63.
94. Leu K, Pope WB, Cloughesy TF, et al. Imaging biomarkers for antiangiogenic therapy in malignant gliomas. CNS Oncol 2013;2:33-47.
95. Nowosielski M, Wiestler B, Goebel G, et al. Progression types after antiangiogenic therapy are related to outcome in recurrent glioblastoma. Neurology 2014;82:1684-92.
96. Kickingereder P, Radbruch A, Burth S. MR Perfusion-derived Hemodynamic Parametric Response Mapping of Bevacizumab Efficacy in Recurrent Glioblastoma. Radiology 2016;279:542-52.
97. Zhang W, Kreisl T, Solomon J, et al. Acute effects of bevacizumab on glioblastoma vascularity assessed with DCE-MRI and relation to patient survival. Proceedings of the Seventeenth Meeting of the International Society for Magnetic Resonance in Medicine. Berkeley, Calif, 2009.
98. Schmainda KM, Prah M, Connelly J, et al. Dynamic-susceptibility contrast agent MRI measures of relative cerebral blood volume predict response to bevacizumab in recurrent high-grade glioma. Neuro-oncol 2014;16:880-8.
99. Kickingereder P, Wiestler B, Burth S, et al. Relative cerebral blood volume is a potential predictive imaging biomarker of bevacizumab efficacy in recurrent glioblastoma. Neuro-oncol 2015;17:1139-47.
100. Ellingson BM, Zaw T, Cloughesy TF, et al. Comparison between intensity normalization techniques for dynamic susceptibility contrast (DSC)-MRI estimates of cerebral blood volume (CBV) in human gliomas. J Magn Reson Imaging 2012;35:1472-7.
101. Flynn JR, Wang L, Gillespie DL, et al. Hypoxia-regulated protein expression, patient characteristics, and preoperative imaging as predictors of survival in adults with glioblastoma multiforme. Cancer 2008;113:1032-42.
102. Ducray F, Idbaih A, Wang XW, et al. Predictive and Prognostic Factors for Gliomas. Expert Rev Anticancer Ther 2011;11:781-9.
103. Yao Y, Kubota T, Takeuchi H, et al. Prognostic significance of microvessel density determined by an anti-CD105/endoglin monoclonal antibody in astrocytic tumors: comparison with an anti-CD31 monoclonal antibody. Neuropathology 2005;25:201-6.
104. Colman H, Giannini C, Huang L, et al. Assessment and prognostic significance of mitotic index using the mitosis marker phosphohistone H3 in low and intermediate-grade infiltrating astrocytomas. Am J Surg Pathol 2006;30:657-64.
105. Patankar TF, Haroon HA, Mills SJ, et al. Is volume transfer coefficient (K(trans)) related to histologic grade in human gliomas? AJNR Am J Neuroradiol 2005;26:2455-65.
106. Law M, Young RJ, Babb JS, et al. Gliomas: predicting time to progression or survival with cerebral blood volume measurements at dynamic susceptibility-weighted contrast-enhanced perfusion MR imaging. Radiology 2008;247:490-8.
107. Mills SJ, Patankar TA, Haroon HA, et al. Do cerebral blood volume and contrast transfer coefficient predict

prognosis in human glioma? AJNR Am J Neuroradiol 2006;27:853-58.
108. Mills SJ, du Plessis D, Pal P, et al. Mitotic Activity in Glioblastoma Correlates with Estimated Extravascular Extracellular Space Derived from Dynamic Contrast-Enhanced MR Imaging. AJNR Am J Neuroradiol 2016;37:811-7.

doi: 10.21037/jxym.2017.06.01
Cite this article as: Lavra F, Scartozzi M, Zaccagna F, Cartocci G, Saba L. Advanced magnetic resonance imaging in the study of primary intracranial brain tumors in adults: a state of art review. J Xiangya Med 2017;2:56.

